Journal of Environmental Chemical Engineering 2 (2014) 2344–2351

Contents lists available at ScienceDirect

Journal of Environmental Chemical Engineering

journal homepage: www.elsevier.com/locate/jece

Adsorption of crystal violet on montmorillonite (or iron modified montmorillonite) followed by degradation through Fenton or photo-Fenton type reactions

L. Guz [a,*], G. Curutchet [a], R.M. Torres Sánchez [b], R. Candal [a,c]

[a] Instituto de Ingenieria e Investigación Ambiental, UNSAM, Av. 25 de Mayo y Francia, 1650 General San Martín, Provincia de Buenos Aires, Argentina
[b] Centro de Tecnología de recursos Minerales y Cerámica-CONICET, Camino Centenario y 506, 1897 M.B. Gonnet, Provincia de Buenos Aires, Argentina
[c] Instituto de Química física de Materiales Ambiente y Energía-CONICET, Pabellón 2, Piso 3, Ciudad Universitaria, 1428 Ciudad Autónoma de Buenos Aires, Argentina

ARTICLE INFO

Article history:
Received 22 November 2013
Received in revised form 10 February 2014
Accepted 11 February 2014
Available online 21 February 2014

Keywords:
Montmorillonite
Adsorption
Fenton
Photo-Fenton
Crystal violet

ABSTRACT

In this work we demonstrate the feasibility to couple adsorption with Fenton and photo-Fenton process to separate and mineralize crystal violet (CV) dissolved in water. Montmorillonite (MMT) and iron modified montmorillonite (MMT-Fe) were studied as adsorbents and heterogeneous catalysts for Fenton and photo-Fenton like oxidation of cationic dye CV. The clays were characterized by XRD, SEM, EDX, BET surface area and electrophoretic mobility. MMT-Fe presents iron in the interlayer space and oxohydroxide particles on its surface. Both clays present a high CV adsorption capacity that can be modeled by a two-site Langmuir equation. MMT-Fe oxidizes faster and have a higher mineralization rate of adsorbed CV than MMT with Fe(II) or Fe(III) added externally. The oxidation of the adsorbed dye release organics to the solution which are further mineralized in solution. The Fenton oxidation can be modeled by a double exponential decay and photo-Fenton oxidation by a pseudo-first order kinetic model. Photo-Fenton oxidation leads to higher mineralization rates than Fenton.

Introduction

Waste water treatment is one of the environmental problems that concern the modern industrial society. In particular, the disposition of colored effluents produced by textile, paper pulp, plastic and other industries represent a technological problem that affects several countries all around the world. It is difficult to calculate the annual amount of waste produced by these industries but some estimates indicate that there are over 100,000 types of synthetic dyes available in the market with an output of 7×10^5 tons per year, and approximately 5–10% is discarded during their production and utilization [1–3]. There are several types of commercial dyes [1,4], and some of these dyes posses a high resistance to biodegradation and persist a long time in the environment [5–7]. These compounds and their degradation byproducts are generally believed to be carcinogenic or toxic and become harmful to humans or to the environment where they are discarded [8–13] and are easily detectable with the naked eye at very low concentrations. Triarylmethane dyes (TAM) are recalcitrant dyes that have been used as antimicrobial and antifungal agents [14–16]. These compounds typically display a net positive charge, being crystal violet (one of the best known members of this family of compounds) a good model to represent cationic dyes.

Adsorption processes have been proposed as a fast alternative to remove contaminants from water. Several natural low cost adsorbents have been tested to remove synthetic dyes [3,17]. In particular, montmorillonite (a clay belonging to the family of smectites) have been broadly studied as adsorbents of synthetic dyes [18–20]. Smectite clays have a layered structure where each layer is composed by tetrahedral silicate units fused into an edge-shared octahedral plane of aluminum. The isomorphic substitution of Al(III) for Fe(II) or Mg(II) and Si(IV) for Al(III) generates charge deficiencies on the surface and interlayer space. When Al(III) is replaced by Mg(II) the structure corresponds to montmorillonite (MMT). The intrinsic negative charge is compensated with inorganic cations (as Na(I) or Ca(II) in MMT) in the interlayer that can be exchanged by other inorganic or organic cations, being suitable for adsorption of cationic synthetic dyes. However, after adsorption and separation from the aqueous effluent a new solid

* Corresponding author. Tel.: +54 1140061500.
E-mail addresses: guzlucas@yahoo.com.ar (L. Guz), gcurut@gmail.com (G. Curutchet), rosa.torres@gmail.com (R.M. Torres Sánchez), rjcandal@gmail.com (R. Candal).

http://dx.doi.org/10.1016/j.jece.2014.02.007
2213-3437/

residue containing the dye is generated. This waste, rich in poorly biodegradable dye, should be adequately disposed as a dangerous solid.

Another alternative to decontaminate dye containing waters are advanced oxidation treatments (AOTs). AOTs are highly efficient treatments to remove recalcitrant dyes based on the oxidative power of the radical species formed. In particular, Fenton and photo-Fenton like processes have proved to be efficient in the oxidation of organic compounds [21,22] using homogeneous iron [23,24], heterogeneous insoluble iron oxides [25,26] or supporting the catalyst in matrixes like clays [27,28]. The Fenton reaction is based in the capacity of Fe(II) to generate hydroxyl radicals from H_2O_2.

$$Fe(II) + H_2O_2 \rightarrow Fe(III) + OH^{\bullet} + OH^{-} \quad (1)$$

These hydroxyl radicals are highly oxidative and can generate chain reactions with organic matter that leads to the mineralization of contaminants. Fe(II) acts as a catalyst and is regenerated from Fe(III), generating even more radicals.

$$Fe(III) + H_2O_2 \rightarrow Fe(III)\text{-}OOH^{2+} + H^{+} \quad (2)$$

$$Fe(III)\text{-}OOH^{2+} \rightarrow Fe(II) + HO_2^{\bullet} \quad (3)$$

In water, Fe(III) undergoes several hydrolysis reactions. At pH 3 almost all Fe(III) is in the form of $Fe(OH)^{2+}$ [29]. This iron complex can absorb light in a broad irradiance spectrum, leading to the photoreduction of Fe(III) [30].

$$Fe(III) + H_2O \rightarrow Fe(III)(OH)^{2+} + H^{+} \quad (4)$$

$$Fe(III)(OH)^{2+} + h\nu \rightarrow Fe(II) + HO^{\bullet} \quad (5)$$

This reaction accelerates the regeneration of Fe(II) from Fe(III), increasing the efficiency of hydroxyl radical production and the reaction velocity. The complex between Fe(III) and H_2O_2 also absorbs polychromatic light leading to the formation of an excited state that accelerates the reduction of Fe(III) [30].

$$Fe(III)\text{-}OOH^{2+} + h\nu \rightarrow Fe(III)\text{-}OOH^{2+}* \rightarrow Fe(II) + HO_2^{\bullet} \quad (6)$$

This light assisted Fenton reaction is commonly known as photo-Fenton reaction.

In this work we propose to use the high adsorption capacity of pure montmorillonite (MMT) and iron modified montmorillonite (MMT-Fe) to remove crystal violet, a model TAM dye, from water and then use homogeneous and heterogeneous Fenton and photo-Fenton like processes to oxidize the adsorbed dye. In this way the dye can be quickly removed from water and concentrated in a smaller volume of water-clay suspensions to be treated.

Materials and methods

Synthesis and characterization of MMT-Fe

MMT-Fe was prepared from Argentinean natural bentonites (MMT), containing 96% of sodium montmorillonite (MMT-Na) (more details in Ref. [31]). MMT-Fe was prepared following the procedures indicated elsewhere [32,33]. Briefly, 300 g/L of MMT were dispersed in acetone containing 1.11 mol/L $FeCl_3$. The dispersion was stirred for 2 h and centrifuge at 10,000 G to separate the solid phase. The solid was rinse with acetone, ethanol and water in this order, followed by centrifugation after each step. Finally, the solid was lyophilized.

The morphology of MMT and MMT-Fe was determined by scanning electron microscopy (SEM) with a FEG-SEM Zeiss Supra 40. The crystalline structure of the samples was determined by X-ray diffraction (XRD) with a Siemens D5000, CuKα radiation, operated at 30 mA and 40 kV. Electrophoretic mobility of MMT and MMT-Fe dispersed in 1 mM KCl solution was determined with a Brookhaven 90 Plus/Bi-MAS. Iron content in MMT and MMT-Fe was determined by dispersing 1 g/L of the sample in exactly 100.0 mL of 5 M nitric acid during 24 h. The concentration of iron in the acid solution was determined by atomic absorption spectroscopy (SensAA dual, GBC Sci. Equipment). Surface area and porosity was determined by adsorption of N_2 at 77 K using a Micromeritics ASAP 2020 V3.05 G. The samples were out-gassed by heating at 200 °C under a flow of helium for 12 h. The data were recorded with P/P_0 between 0.0005 and 0.99.

Adsorption isotherms

1.5 g/L of MMT or MMT-Fe were dispersed in water solutions containing crystal violet (CV) concentrations in the range 0.245–2.45 mM. The dispersion was stirred during 24 h to equilibrate the system and then centrifuge at 10,000 G during 15 min. The concentration of the dye remaining in solution was measured by UV–vis spectroscopy (PG Instruments T70+).

Determination of the adsorbed dye

To determine the amount of CV adsorbed on MMT or MMT-Fe, the dye was desorbed by treatment with an aqueous solution of sodium dodecyl sulfate (SDS). The desorbed dye was quantified by UV–vis spectroscopy in the extractive solution. To optimize the extraction of CV from MMT, the following procedure was realized: 0.15 g/L of MMT or MMT-Fe were dispersed in 100 mL of 0.060 mM CV solution and stirred during 3 h; the solid was separate by centrifugation at 10,000 G during 15 min and resuspended in 100 mL of water solutions containing different concentration of SDS. The optimum concentration of SDS to remove all the dye from the adsorbent was 0.17 M (see supplementary Fig. 1).

Supplementary material related to this article can be found, in the online version, at doi:10.1016/j.jece.2014.02.007.

Fenton and photo-Fenton reaction set-up

To simulate the removal of pollutants in water by adsorption followed by advanced oxidation, CV was first adsorbed on MMT (or MMT-Fe), separated from the water and re-dispersed in a lower amount of water, were it was oxidized by Fenton or photo-Fenton process. The experimental procedure can be summarized as follows: 100 mL 0.060 mM CV were stirred during 24 h with 1.5 g/L MMT (or MMT-Fe) to reach adsorption equilibrium condition. The sorbent/sorbate system was separated from solution by centrifugation at 10,000 G. The solid was re suspended in 50 mL of water at pH 3.0 (acidify with H_2SO_4). The suspension was placed in a 100 mL double jacket borosilicate glass batch reactor, thermostated at 25 °C and magnetically stirred. Enough 30% H_2O_2 to reach a final concentration of 50 mM was added as oxidant and, for the system with MMT, 0.5 mM $FeCl_3$ or $Fe(NH_4)_2(SO_4)_2$ was added as catalyst [24]. For photo-Fenton experiments, the reactor was illuminated from above with a 300 W solar lamp (OSRAM, Ultravitalux). 5 mL samples were taken from the reactor at fixed times, quenched with sodium sulfite or acetonitrile, and centrifuged at 10,000 G to remove the adsorbent. Total Organic Carbon (TOC) and iron concentration were measured in the supernatant solution using a Shimadzu TOC-5000 and an atomic absorption spectrophotometer SensAA dual, GBC Sci equipment, respectively. The dye was desorbed from the adsorbent with a 0.17 M sodium dodecyl sulfate water solution. The concentration of the extracted dye was measured by UV–vis spectrophotometry. Details about the extraction procedure are given as supplementary material.

Results and discussion

Catalysts characterization

Fig. 1A and B shows SEM images of MMT and MMT-Fe samples respectively. The images show that the particles were formed by aggregates of montmorillonite layers. In the case of MMT-Fe, some prismatic shaped nanoparticles can be seen on the surface (marked with white circles).

EDX analysis (Table 1) indicates that MMT-Fe was enriched in iron, suggesting that the prismatic particles may be formed by a rich iron phase.

By comparing EDX analysis of both MMT and MMT-Fe samples it can be noticed that sodium is not present in MMT-Fe, which may be consequence of the exchange of Fe(III) by Na cations as reported before [34]. These results indicates that Fe(III) was partially deposited on the particles, probably as iron oxohydroxide, and partially located inside the clay interlayer space after exchange with the interlayer located Na(I). Fig. 2 shows XRD patterns of MMT and MMT-Fe samples. It is clear that the interlayer space, evaluated by the reflexion peak *d* 0 0 1 increased from 13.6 A to 16.5 A when Fe(III) was added to MMT. The increment of the interlayer space indicates that part of the Fe(III) was incorporated into the aluminosilicate layers that form the MMT structure. Reports regarding the effect of Fe(III) on interlayer space in MMT samples are varied. Some authors found a small decrease in the interlayer space when Fe(III) was incorporated to MMT, which was attributed to the smaller radius of $[Fe(H_2O)_6]^{3+}$ with respect to Na cation [35]. Other authors reported a slight increase in the reflexion peak *d* 0 0 1 attributed to the presence of polymeric species of Fe(III) within the interlayer [36]. Luengo et al. reported the broadening of the *d* 0 0 1 reflection peak in MMT-Fe sample prepared in similar way than that used in this work. The broadening was assigned to disorganization of the staking of layers [37]. The last authors also reported the presence of Fe(III) on the surface of the Fe-MMT particles. These results agree with ours, which are supported by EDX analysis as discussed above.

Table 1
Elemental composition of MMT and MMT-Fe samples determined by EDX.

Element	MMT		MMT-Fe	
	% weight	% atomic	% weight	% atomic
C	11.52	17.96	8.11	13.97
O	46.67	54.64	42.19	54.18
Na	1.28	1.04	0	0
Mg	1.23	0.95	1.41	1.20
Al	16.11	11.18	10.24	7.85
Si	19.43	12.96	23.80	17.18
Fe	3.77	1.26	14.25	5.28

Fig. 3 shows zeta potential values vs pH for both MMT and MMT-Fe samples. The zeta potential of MMT sample remained almost constant with pH, as typical for this type of clays in which the surface charge is always negative due to the isomorphous substitution, indicated previously. In the case of MMT-Fe sample the zeta potential changed with the pH, increasing as the pH decreased. This behavior may be related to the presence of Fe(III) oxohydroxide nanoparticles on the surface of the clay aggregates, as revealed by SEM and EDX analysis. Iron oxohydroxides, as goethite have isoelectric point close to pH 8 and its zeta potential change with pH. The presence of Fe(III) species on the surface modify the charge and the surface properties of the original material.

The iron content of both samples was determined by extraction with concentrated nitric acid and measured by atomic absorption. MMT and MMT-Fe samples have 0.25 ± 0.02 and 0.9 ± 0.1 mmol Fe/g of clay, respectively. These values are lower than those obtained by EDX. However, the iron ratio between MMT-Fe and MMT determined by both techniques is very similar, indicating that MMT-Fe has approximately 3.7 times more iron than MMT. It should be mentioned that EDX is a surface characterization technique. Consequently the higher percentage of iron determined by EDX indicates that most of Fe is located at the surface, very likely in the form of iron oxides nanoparticles, as shown in Fig. 1A and B.

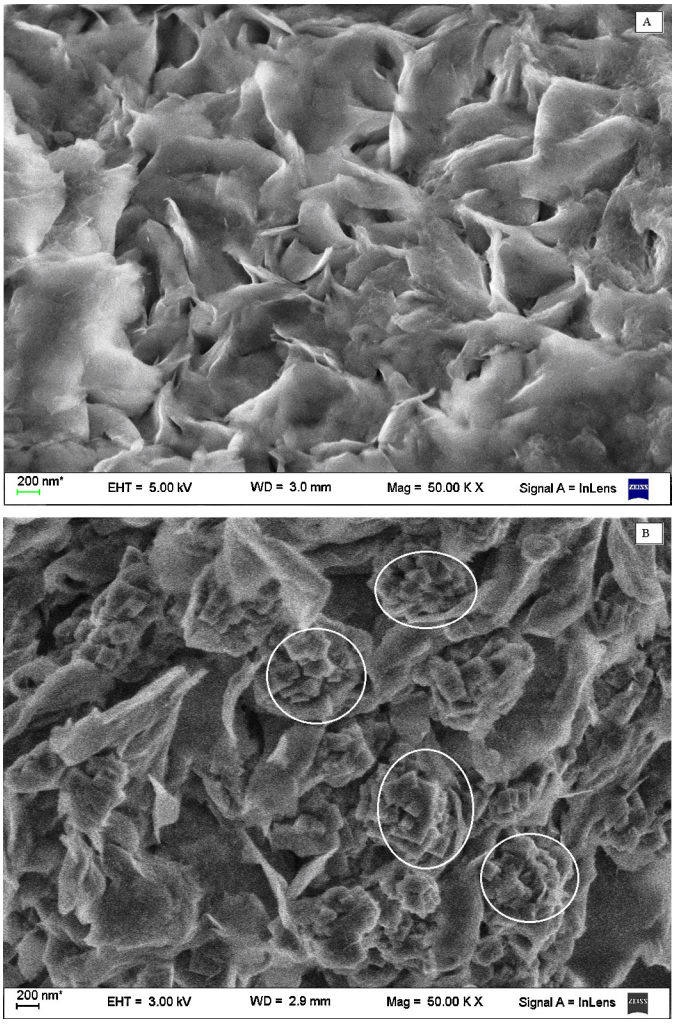

Fig. 1. SEM images of MMT (A) and MMT-Fe (B) samples.

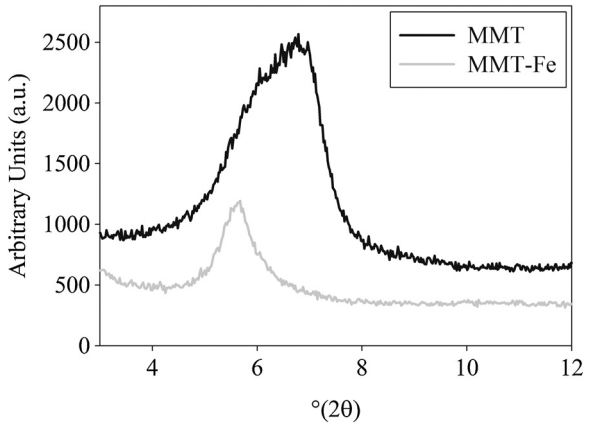

Fig. 2. XRD analysis of MMT and MMT-Fe samples.

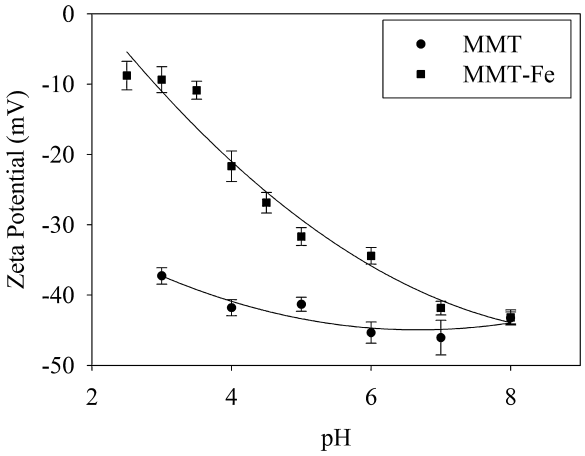

Fig. 3. Effect of pH on zeta potential in MMT and MMT-Fe.

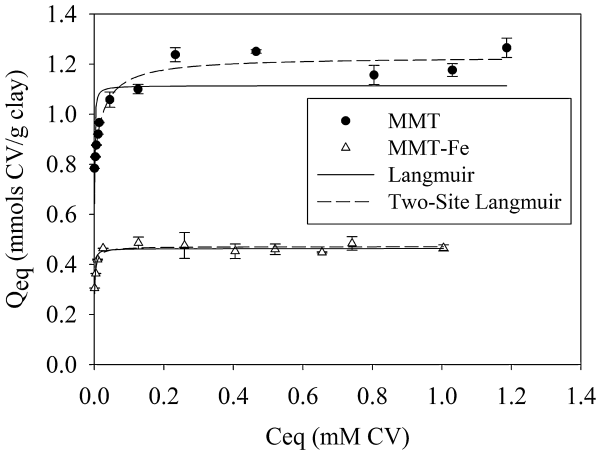

Fig. 4. Adsorption isotherms of CV on MMT and MMT-Fe.

Table 2
BET surface area and micropore structure parameters.

	BET surface (m^2/g)	Wp (average pore width) (Å)	Total pore volume (cm^3/g)
MMT	56	22	0.06
MMT-Fe	46	19	0.04

Table 2 shows the BET surface area and microstructure characteristics of both clays. The adsorption isotherms of both materials belong to the Type II isotherm type with a very important type H_3 hysteresis loop, which demonstrate the mesoporous structure of the material, which is typical of this kind of clays [38] (see Supplementary Fig. 2). The presence of Fe(III) decreases the BET surface area and porosity of MMT-Fe. Very likely this phenomenon is a consequence of the growing of iron oxides nanoparticles at the surface and into the interlayer space, diminishing the pore diameter and the overall porosity. The area of MMT is 18% bigger than MMT-Fe.

Supplementary material related to this article can be found, in the online version, at doi:10.1016/j.jece.2014.02.007.

As conclusion of the characterization results, it is clear that Fe(III) is located into the interlayer space and at the surface of the MMT particles (very likely in the form of oxohydroxide particles). A good distribution of the nanoparticles is promissory for the application of this material as heterogeneous catalyst in photo-Fenton like processes.

Adsorption of CV on MMT and MMT-Fe

Fig. 4 shows adsorption isotherms of CV on MMT and MMT-Fe. The adsorption of CV on MMT follows a Langmuir like behavior that can be better fitted by a two sites model (Eq. (7)) than by a simple Langmuir model.

$$Q_{eq} = \frac{Q_{max1} \times C_{eq}}{K_{d1} + C_{eq}} + \frac{Q_{max2} \times C_{eq}}{K_{d2} + C_{eq}} \quad (7)$$

Q_{maxi} and K_{di} in Eq. (7) represent the highest adsorption capacity and desorption constants of CV on site i respectively [39]. The results obtained from the fitting are shown in Table 3.

The maximum amount of CV adsorbed on MMT (1.23 mmol/g) is in the range reported in the literature [19,20]. The two site model indicates the presence of two principal sites that display different highest adsorption capacities and desorption constant. Although more insight into the characteristics of the sites may be speculative, the presence of sites with different adsorption capacities on these types of solids is not rare due to the existence of borders, steps and defects on the surface of the particles.

In the case of MMT-Fe the highest adsorption capacity of CV was lower than for MMT. This result was expected due to the following reasons. Firstly, the experiment was run at pH 3.5 and, as reported by Monash [19] the adsorption of CV on clays decreases with the pH. This effect can be explained as a consequence of the competition of H^+ by the negative sites on the surface. Secondly MMT-Fe displayed a lower BET surface area and porosity than MMT, very likely leading to a diminution in the adsorption capacity. Finally, the presence of Fe(III) on the surface shifted the zeta potential to more positive values, being this effect very remarkable at pH 3 (see Fig. 3). Consequently a reduction in CV adsorption was expected. The isotherm curve can be fitted by a simple Langmuir equation, indicating that the sites available for CV adsorption had similar behavior. This characteristics may be consequence of the well distribution of Fe(III) on the surface; very likely only the sites on the flat surface of the flakes are available for CV being the borders, corners and junctions between flakes occupied by Fe(III) nanoparticles (see Fig. 1).

Fenton and photo-Fenton treatment

Based on the adsorption parameters obtained with the two-site Langmuir model shown in Table 3, under the experimental conditions used in the adsorption experiments previous to the Fenton and photo-Fenton experiments, 99.997% and 99.906% of the initial CV was adsorbed on MMT and MMT-Fe respectively. From a practical point of view, CV was completely removed from the

Table 3
Isotherm parameters for crystal violet on MMT and MMT-Fe.

	R^2	Q_{max1} (mmol/g)	K_{d1}	Q_{max2} (mmol/g)	K_{d2}
MMT	0.9519	0.80 ± 0.07	$2.5 \times 10^{-5} \pm 0.1 \times 10^{-5}$	0.43 ± 0.06	0.03 ± 0.01
MMT-Fe	0.9321	0.25 ± 0.03	$2.0 \times 10^{-4} \pm 5 \times 10^{-5}$	0.21 ± 0.03	$0.003 \pm 5 \times 10^{-4}$

solution, being the supernatant completely transparent and CV not detectable by UV–vis spectrophotometry. By the other hand, MMT or MMT-Fe became dark violet due to the adsorption of CV. TOC measurements indicate that the concentration of organics remaining in solution were similar to those obtained by suspending the clays in distilled water. It should be noticed that the clays release organics to the aqueous media, at a rate of 0.77 mg C/g MMT and 1.43 mg C/g MMT-Fe at pH 5.5. At lower pH the clays release even more organics, increasing to 3.2 mg C/g MMT and 5.0 mg C/g MMT-Fe at pH 3. Natural clays always have organic matter in its composition. In the case of MMT-Fe, the higher content of organics might be consequence of the presence of traces of ethanol used in its preparation.

During Fenton like treatments the solution remained colorless meaning that CV was not released to the solution. However the color of the clays changed from dark violet to its original pale brown color, indicating that the adsorbed dye was decolorized during the treatment. The degradation of CV in solution by Fenton and Fenton-like reaction was reported before [24], but there are not reports of the degradation of CV adsorbed on clays. Fig. 5 shows the temporal evolution of CV adsorbed on MMT or MMT-Fe during different Fenton like treatments in terms of C/C_0, where C_0 is the concentration of CV in the extractive solution at $t = 0$ and C is the concentration at any other time (details are given in the experimental methods and supplementary material).

In the system containing only MMT and adsorbed CV, the incorporation of H_2O_2 produced only a slight discoloration of CV. However, when Fe(II) or Fe(III) were added to the solution CV was clearly degraded. Fe(II) displayed more activity than Fe(III) as was reported for homogeneous Fenton reaction. By the other hand in the system containing CV adsorbed on MMT-Fe, CV was faster degraded after H_2O_2 incorporation than in the previous cases.

Table 4 shows the concentration of total iron in solution (irrespective of the oxidation state) at the beginning and at the end of the experiments. The results indicate that when Fe(II) or Fe(III) were incorporated to the system containing MMT and CV, 74/% of the added iron was immediately adsorbed on the clay, being the concentration of iron remaining in solution 0.13 mM. In the case of MMT-Fe, 4% of the total iron was leached to the solution being the remaining concentration of Fe(III) approximately 0.17 mM during all the experiment. It should be notice that the concentration of iron in solution was quite similar in all the experiments and it was not negligible. In other words, an important contribution of homogeneous Fenton reaction is expected in all the cases. Unfortunately, the contribution of homogeneous Fenton is not easily quantifiable because in this case CV is completely adsorbed at the surface of the solid, and it is not comparable with the case where CV is dissolved in water (see Supplementary Fig. 3). However, the concentration of iron in solution is too similar in all the cases and cannot explain the differences in discoloration rate. Clearly, there is an important role of the Fe(III) deposited on the surface of MMT-Fe in the degradation process of CV.

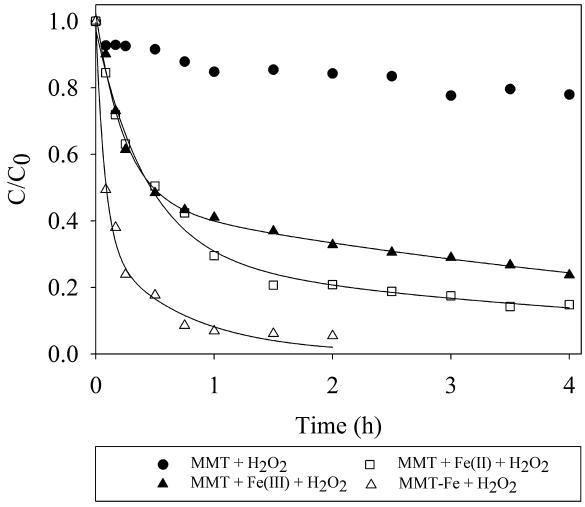

Fig. 5. Degradation of adsorbed CV on MMT, MMT+Fe(III), MMT+Fe(II) and MMT-Fe by Fenton. [H_2O_2] = 50 mM, pH 3, [Fe(II)] and [Fe(III)] = 0.5 mM, MMT and MMT-Fe 3 g/L, [CV] = 0.120 mM.

Table 4
Concentration of iron in solution after 0 and 4 h of Fenton treatment.

$[Fe]_T$	T = 0 h (mM)	T = 4 h (mM)
MMT	0.022	0.058
MMT+Fe(II)	0.13	0.13
MMT+Fe(III)	0.13	0.13
MMT-Fe	0.17	0.16

Supplementary material related to this article can be found, in the online version, at doi:10.1016/j.jece.2014.02.007.

Table 5 displays the kinetics parameters obtained from the experimental data shown in Fig. 5 after fitting with a double exponential equation:

$$\frac{C}{C_0} = a \times e^{-k_1 t} + b \times e^{-k_2 t} \quad (8)$$

A double exponential kinetic equation may be consequence of different possible mechanism. Gordon et al. proposed a two step pseudo-first order reaction for heterogeneous Fenton reaction [40]. In his model, the dissolved homogeneous iron and the surface heterogeneous iron have different velocity constant for the production of hydroxyl radicals, leading to two parallel degradation reactions for 2-chlorophenol. In our heterogeneous system, iron was released to the solution in MMT-Fe and adsorbed to the surface of MMT when added homogeneously (Table 3), leading to a combination of homogeneous and heterogeneous Fenton degradation process (Reactions (2), (3) and (9) and (10)). Chen and Zhu also reported that the leaching of iron by different Fe-pillared bentonites leads to a simultaneous heterogeneous and homogeneous dye degradation, helping in the final mineralization of the organic byproducts present in water [41].

$$\equiv Fe(III) + H_2O_2 \rightarrow \equiv FeOOH^{2+} + H^+ \quad (9)$$

$$\equiv Fe(III)\text{-}OOH^{2+} \rightarrow \equiv Fe(II) + OH_2^{\bullet} \quad (10)$$

Other authors also propose a double exponential equation with different kinetic constants, one fast and one slow, for degradation of organics by Fenton's reaction [42–44]. In this kinetic model, the two exponential decays corresponds to the formation of radicals from H_2O_2 by Fe(II) (fast, Reactions (1) and (11)) and by Fe(III) (slow, Reactions (2), (3) and (9) and (10)).

$$\equiv Fe(III)\text{-}H_2O_2 \rightarrow \equiv Fe(III) + HO^{\bullet} + OH^- \quad (11)$$

Reactions (10) and (11) may explain the active role of Fe(III) attached on MMT-Fe on the discoloration of adsorbed CV. These reactions illustrate the production of $HO^{\bullet}$ radicals at the surface of MMT-Fe. Considering that CV is adsorbed at the surface of MMT-Fe

Table 5
Kinetic parameters for the degradation of CV adsorbed on MMT or MMT-Fe by Fenton process. pH = 3.0; [H_2O_2] = 50 mM, T = 25 °C.

	R^2	a	k_1 (h^{-1})	b	k_2 (h^{-1})
MMT+Fe(II)	0.9931	0.68 ± 0.07	2.31 ± 0.4	0.29 ± 0.07	0.19 ± 0.09
MMT+Fe(III)	0.9946	0.57 ± 0.03	4.1 ± 0.5	0.46 ± 0.03	0.16 ± 0.02
MMT-Fe	0.9927	0.67 ± 0.09	13.3 ± 3.4	0.33 ± 0.09	1.4 ± 0.4

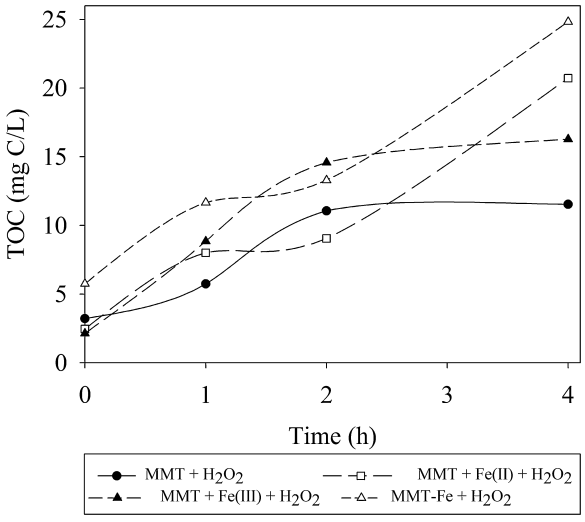

Fig. 6. TOC removal by Fenton experiments.

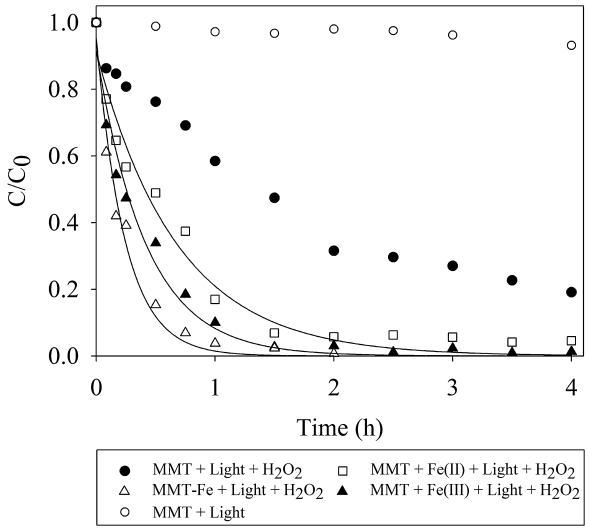

Fig. 7. Degradation of adsorbed CV on MMT, MMT+Fe(III), MMT+Fe(II) and MMT-Fe by Fenton. [H_2O_2] = 50 mM, pH 3, [Fe(II)] and [Fe(III)] = 0.5 mM, MMT and MMT-Fe 3 g/L, [CV] = 0.120 mM, visible light: 1.5×10^{18} photons/s at 366 nm.

and there is not CV in solution, very likely the HO• radicals produced at the level of the surface will act more efficiently in CV degradation than those generated in the solution bulk. MMT-Fe has a higher concentration of Fe(III) at the surface than the other systems (where Fe(III) or Fe(II) were incorporated to the solution) and consequently a higher production of HO• at the surface is expected.

As it was mentioned before, the concentration of Fe(II)/Fe(III) in solution is not negligible and homogeneous Fenton reactions are expected. But the target of this process would likely be the byproducts released to solution. Fig. 6 shows the temporal evolution of TOC in water, in all the cases TOC increased with the time as CV was discolored at the surface of the adsorbent (see Fig. 5). These results indicate that CV was not immediately mineralized and the byproducts were detached from the surface and released to the solution. Once in solution, these byproducts may be further oxidized by homogeneous Fenton reactions, due to the presence of Fe(III)/Fe(II) and H_2O_2 in solution. The results show that the oxidation rate in solution was slower than at the surface of the clays and the organics were accumulated in solution.

Table 6 displays the percentage of CV oxidized, the maximum TOC expected in solution assuming that CV is not mineralized, the measured TOC and the percentage of mineralization assuming all the organics were removed from the adsorbent. MMT-Fe is the most effective catalyst because CV is almost completely eliminated from the adsorbent and 42% of the TOC was mineralized.

To the best of our knowledge, photo-Fenton degradation of CV has not been reported. To confirm the feasibility to degrade CV by photo-Fenton reaction, a preliminary experiment with dissolved CV was performed. The results clearly indicate that CV can be discolored by photo-Fenton reaction (Supplementary Fig. 3). Fig. 7 shows the temporal evolution of CV adsorbed on MMT or MMT-Fe during photo-Fenton treatment. As in Fenton treatment, the solution remained colorless during all the experiment for all the cases.

By comparing Fig. 7 with Fig. 5 it is clear that the application of light improved the discoloration rate in all the studied cases. The application of light alone did not degrade CV but when H_2O_2 was incorporated to the system the combination of light and H_2O_2 leaded to partial discoloration of the adsorbed CV. This phenomenon may be associated with the presence of small amounts of Fe(III) on natural MMT and to the activation of the dye by absorption of light. The exited dye may react with H_2O_2 leading to discoloration. When Fe(II) or Fe(III) were added to the suspensions containing MMT and adsorbed CV, the discoloration rate was notably improved. It is interesting to note that in this case Fe(III) resulted more active than Fe(II), in opposition to the result obtained during Fenton treatment. This result is in agreement with the proposed mechanism for photo-Fenton that involve the generation of HO• radicals by photochemical decomposition of Fe(III) hydroxo complex [27]:

$$Fe(III)(OH)^{2+} + h\nu \rightarrow Fe(II) + HO^{\bullet} \quad (5)$$

In the case of MMT-Fe the discoloration rate was even higher than in the previous cases. Supported Fe(III) may generate HO• radicals by UVA–visible illumination according to Reaction (12) [45]:

$$\equiv Fe(III)\text{-}(OH)^{2+} + h\nu \rightarrow \equiv Fe(III)(OH)^{2+}* \rightarrow \equiv Fe(II) + OH^{\bullet} \quad (12)$$

As was discussed before for Fenton reaction, HO• generated at the surface may play a predominant role in the oxidation of

Table 6
TOC and mineralization percentage.

System	% CV oxidized $t = 4$ h	TOC (ppm) $t = 0$	TOC (ppm) $t = 4$ h	TOC[1] (ppm) Corrected	TOC[2] (ppm) Maximum	% mineralization[3]
MMT	20	3	11	8	7.2	0
MMT+Fe(III)	70	2	16	14	25.2	44
MMT+Fe(II)	82	2	21	19	29.5	35.6
MMT-Fe	95	5	25	20	34.2	41.5

[1] TOC corrected = [TOC ($t = 4$ h)] − [TOC ($t = 0$)].
[2] Theoretical TOC corresponding to oxidized CV released to the solution (50 ppm of CV = 36 ppm TOC).
[3] % mineralization = $100 \times [TOC^2 - TOC^1]/TOC^2$.

Table 7
Parameter for the degradation of CV adsorbed on MMT or Fe-MMT by photo-Fenton process. pH = 3.0; $[H_2O_2] = 50$ mM, $T = 25$ °C, light source 1.5×10^{18} photons/s at 366 nm.

	R^2	K (h^{-1})
MMT+Fe(II)	0.9732	1.5 ± 0.1
MMT+Fe(III)	0.9817	2.4 ± 0.2
MMT-Fe	0.9833	4.2 ± 0.4

adsorbed CV. Due to the high amount of Fe(III) available at the surface of MMT-Fe, higher discoloration rate of adsorbed CV with respect to all the other cases is expected.

Table 7 shows the kinetic parameters obtained by fitting of the experimental data with a simple exponential equation.

The discoloration curves of the systems containing extra iron could be fitted by a pseudo first order rate equation. The reasons of the differences with the Fenton case are not clear, but it may be consequence of the high constant rate of Reactions (4) and (10) for the regeneration of Fe(II) in comparison to Reactions (2), (3) and (9) and (10) [22,27]. Under illumination Fe(III) is faster reduced to Fe(II) than in the dark and this step is not any more limiting the reaction rate. The constant rates are parametric in iron concentration and H_2O_2 concentration; the different values are only indicative of the different discoloration rate under the studied conditions. Fig. 8 shows the temporal evolution of TOC.

In the case of CV adsorbed on MMT exposed to light in the presence of H_2O_2 there was a fast an increment in TOC during the first hour, followed by a slow increment at longer times. This increment in TOC is related with the degradation of CV on the MMT followed by the release of oxidized byproducts to the solution. It should be noted that the higher TOC expected, based in the mass balance of CV, is 36 ppm. When compared with the TOC reached after 4 h of treatment (24 ppm) it is clear that mineralization was negligible (from Fig. 7, 80% of CV was eliminated which corresponds to a TOC of 28 ppm; only 4 ppm were mineralized). In the other systems, TOC increased during the first hour of treatment but quickly decreased after the first hour. The $HO^{\bullet}$ generated by homogeneous photo-Fenton reaction may be responsible for the mineralization of the oxidation byproducts released to solution after oxidation of the adsorbed CV. As in the Fenton like experiments discussed above (see Table 6), MMT+Fe(III) was the most effective in mineralization of the organics released into the solution, followed by MMT+Fe(II) and MMT-Fe. These results suggest that the iron incorporated to the solution is more available to catalyze the oxidation of the byproducts in solution. This is an interesting phenomenon considering that MMT-Fe is more effective to degrade the adsorbed CV. One of the reasons for this effect could be that the Fe(III) in solution could form complexes with the organic byproducts released to the solution more easily than the Fe(III) adsorbed to MMT. This Fe(III)-organic complexes could produce organic oxidation products in the presence of light by ligand to metal charge transfer [22,26,28]:

$$\text{Fe(III)-R} + h\nu \rightarrow \text{Fe(II)} + R^{+\bullet} \quad (13)$$

The degradation mechanism of CV by Fenton process and the more important oxidized byproducts were recently reported. N-de-methylation and cleavage of the conjugated chromophore structure were the mayor primary mechanism of CV degradation. Aromatic N-methylamines, aldehydes and carboxylic acid were the most important remaining substances [24]. In our case mineralization of organic in solution was more that 90% by using photo-Fenton process.

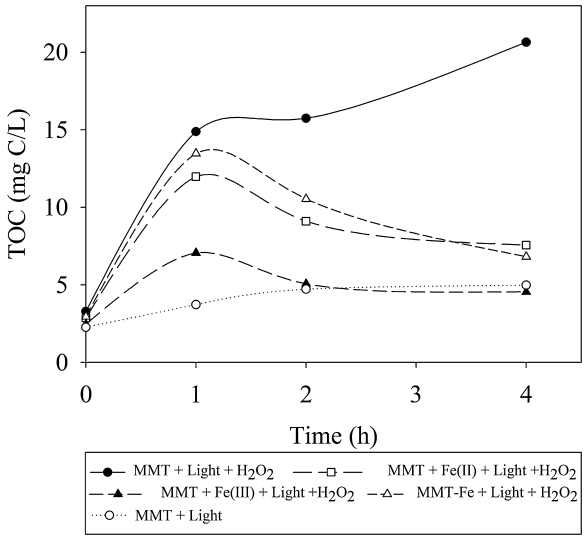

Fig. 8. TOC removal by photo-Fenton experiments.

Conclusions

Absorption of CV on MMT and MMT-Fe indicates that bentonites can be efficiently used to remove intrinsically positive dyes from water. The absorption capacity and the adsorption constant are big enough to allow the removal of relatively high concentrations of dye from water. The adsorbant/sorbate solid can be separated from solution and treated by Fenton or photo-Fenton to thoroughly eliminate the contaminant. In such a way the problem of the safe disposal of the contaminated solid can be resolved. The results presented in this paper show that the contaminant adsorbed at the adsorbent can be oxidized by Fenton or photo-Fenton, being the byproducts released to the solution. Photo-Fenton resulted more efficient to completely mineralize the organics liberated during the adsorbed dye oxidation. MMT-Fe was the most active catalyst for discoloration, being involved in the catalytic process both supported and soluble iron. Our results indicate that the combination of adsorption on clays followed by advanced oxidation is a promissory combination for the removal and destruction of organic contaminants in water.

Acknowledgments

This research was founding by FONARSEC, through FS-NANO 08. R.M.T.S., G.C. and R.C. are members of CONICET. The fellowship granted to L.G. by CONICET is very grateful. The authors thank CETMIC-CONICET and 3iA-UNSAM for all the support given to this project.

References

[1] E. Forgacs, T. Cserháti, G. Oros, Removal of synthetic dyes from wastewaters: a review, Environment International 30 (2004) 953–971.
[2] A.B. dos Santos, F.J. Cervantes, J.B. van Lier, Review paper on current technologies for decolourisation of textile wastewaters: perspectives for anaerobic biotechnology, Bioresource Technology 98 (2007) 2369–2385.
[3] V.K. Gupta, Suhas, Application of low-cost adsorbents for dye removal – a review, Journal of Environmental Management 90 (2009) 2313–2342.
[4] M.A. Rauf, S. Salman Ashraf, Survey of recent trends in biochemically assisted degradation of dyes, Chemical Engineering Journal 209 (2012) 520–530.
[5] A. Paszczynski, M.B. Pasti, S. Goszczynski, D.L. Crawford, R.L. Crawford, New approach to improve degradation of recalcitrant azo dyes by *Streptomyces* spp. and *Phanerochaete chrysosporium*, Enzyme and Microbial Technology 13 (1991) 378–384.
[6] S. Camarero, D. Ibarra, M.J. Martínez, Á.T. Martínez, Lignin-Derived Compounds as Efficient Laccase Mediators for Decolorization of Different Types of Recalcitrant Dyes, 2005, 1775–1784.

[7] G. de Aragão Umbuzeiro, H.S. Freeman, S.H. Warren, D.P. de Oliveira, Y. Terao, T. Watanabe, L.D. Claxton, The contribution of azo dyes to the mutagenic activity of the Cristais River, Chemosphere 60 (2005) 55–64.
[8] P.A. Carneiro, G.A. Umbuzeiro, D.P. Oliveira, M.V.B. Zanoni, Assessment of water contamination caused by a mutagenic textile effluent/dyehouse effluent bearing disperse dyes, Journal of Hazardous Materials 174 (2010) 694–699.
[9] F.M.D. Chequer, T.M. Lizier, R. de Felício, M.V.B. Zanoni, H.M. Debonsi, N.P. Lopes, R. Marcos, D.P. de Oliveira, Analyses of the genotoxic and mutagenic potential of the products formed after the biotransformation of the azo dye Disperse Red 1, Toxicology In Vitro 25 (2011) 2054–2063.
[10] M. Zubair Alam, S. Ahmad, A. Malik, M. Ahmad, Mutagenicity and genotoxicity of tannery effluents used for irrigation at Kanpur, India, Ecotoxicology and Environmental Safety 73 (2010) 1620–1628.
[11] M.I. Beydilli, S.G. Pavlostathis, W.C. Tincher, Decolorization and toxicity screening of selected reactive azo dyes under methanogenic conditions, Water Science and Technology 38 (1998) 225–232.
[12] C. Wang, A. Yediler, D. Lienert, Z. Wang, A. Kettrup, Toxicity evaluation of reactive dyestuffs, auxiliaries and selected effluents in textile finishing industry to luminescent bacteria *Vibrio fischeri*, Chemosphere 46 (2002) 339–344.
[13] K. Golka, S. Kopps, Z.W. Myslak, Carcinogenicity of azo colorants: influence of solubility and bioavailability, Toxicology Letters 151 (2004) 203–210.
[14] J.J. Jones, J.O. Falkinham, Decolorization of Malachite Green and Crystal Violet by Waterborne Pathogenic Mycobacteria, 2003, 2323–2326.
[15] D.J. Alderman, Malachite green: a review, Journal of Fish Diseases 8 (1985) 289–298.
[16] W.C. Andersen, S.B. Turnipseed, C.M. Karbiwnyk, R.H. Lee, S.B. Clark, W.D. Rowe, M.R. Madson, K.E. Miller, Multiresidue method for the triphenylmethane dyes in fish: malachite green, crystal (gentian) violet, and brilliant green, Analytica Chimica Acta 637 (2009) 279–289.
[17] G. Crini, Non-conventional low-cost adsorbents for dye removal: a review, Bioresource Technology 97 (2006) 1061–1085.
[18] X.S. Wang, W. Zhang, Removal of basic dye crystal violet from aqueous solution by Cu(II)-loaded montmorillonite, Separation Science and Technology 46 (2011) 656–663.
[19] P. Monash, G. Pugazhenthi, Removal of crystal violet dye from aqueous solution using calcined and uncalcined mixed clay adsorbents, Separation Science and Technology 45 (2009) 94–104.
[20] J. Wei, R. Zhu, J. Zhu, F. Ge, P. Yuan, H. He, C. Ming, Simultaneous sorption of crystal violet and 2-naphthol to bentonite with different CECs, Journal of Hazardous Materials 166 (2009) 195–199.
[21] E. Neyens, J. Baeyens, A review of classic Fenton's peroxidation as an advanced oxidation technique, Journal of Hazardous Materials 98 (2003) 33–50.
[22] J.J. Pignatello, E. Oliveros, A. MacKay, Advanced oxidation processes for organic contaminant destruction based on the Fenton reaction and related chemistry, Critical Reviews in Environmental Science and Technology 36 (2006) 1–84.
[23] F. Ay, E.C. Catalkaya, F. Kargi, A statistical experiment design approach for advanced oxidation of Direct Red azo-dye by photo-Fenton treatment, Journal of Hazardous Materials 162 (2009) 230–236.
[24] H.-J. Fan, S.-T. Huang, W.-H. Chung, J.-L. Jan, W.-Y. Lin, C.-C. Chen, Degradation pathways of crystal violet by Fenton and Fenton-like systems: condition optimization and intermediate separation and identification, Journal of Hazardous Materials 171 (2009) 1032–1044.
[25] P. Baldrian, V. Merhautová, J. Gabriel, F. Nerud, P. Stopka, M. Hrubý, M.J. Beneš, Decolorization of synthetic dyes by hydrogen peroxide with heterogeneous catalysis by mixed iron oxides, Applied Catalysis B: Environmental 66 (2006) 258–264.
[26] A.N. Soon, B.H. Hameed, Heterogeneous catalytic treatment of synthetic dyes in aqueous media using Fenton and photo-assisted Fenton process, Desalination 269 (2011) 1–16.
[27] J. Herney-Ramirez, M.A. Vicente, L.M. Madeira, Heterogeneous photo-Fenton oxidation with pillared clay-based catalysts for wastewater treatment: a review, Applied Catalysis B: Environmental 98 (2010) 10–26.
[28] Q. Chen, P. Wu, Y. Li, N. Zhu, Z. Dang, Heterogeneous photo-Fenton photodegradation of reactive brilliant orange X-GN over iron-pillared montmorillonite under visible irradiation, Journal of Hazardous Materials 168 (2009) 901–908.
[29] H. Gallard, J. De Laat, B. Legube, Spectrophotometric study of the formation of iron(III)-hydroperoxy complexes in homogeneous aqueous solutions, Water Research 33 (1999) 2929–2936.
[30] S.H. Bossmann, E. Oliveros, S. Göb, S. Siegwart, E.P. Dahlen, L. Payawan, M. Straub, M. Wörner, A.M. Braun, New evidence against hydroxyl radicals as reactive intermediates in the thermal and photochemically enhanced Fenton reactions, Journal of Physical Chemistry A 102 (1998) 5542–5550.
[31] A.P. Magnoli, L. Tallone, C.A.R. Rosa, A.M. Dalcero, S.M. Chiacchiera, R.M. Torres Sanchez, Commercial bentonites as detoxifier of broiler feed contaminated with aflatoxin, Applied Clay Science 40 (2008) 63–71.
[32] A. Komlósi, E. Kuzmann, N.M. Nagy, Z. Homonnay, S. Kubuki, J. Kónya, Incorporation of Fe in the Interlayer of Na-Montmorillonite via Treatment with $FeCl_3$ in Acetone, 2007, 89–95.
[33] T.-S. Li, Z.-H. Zhang, Y.-J. Gao, A rapid preparation of acylals of aldehydes catalysed by Fe^{3+}-montmorillonite, Synthetic Communications 28 (1998) 4665–4671.
[34] D. Nguyen-Thanh, K. Block, T.J. Bandosz, Adsorption of hydrogen sulfide on montmorillonites modified with iron, Chemosphere 59 (2005) 343–353.
[35] L. Borgnino, M.J. Avena, C.P. De Pauli, Synthesis and characterization of Fe(III)-montmorillonites for phosphate adsorption, Colloids and Surfaces A: Physicochemical and Engineering Aspects 341 (2009) 46–52.
[36] J.P. Chen, M.C. Hausladen, R.T. Yang, Delaminated Fe_2O_3-pillared clay: its preparation, characterization, and activities for selective catalytic reduction of NO by NH_3, Journal of Catalysis 151 (1995) 135–146.
[37] C. Luengo, V. Puccia, M. Avena, Arsenate adsorption and desorption kinetics on a Fe(III)-modified montmorillonite, Journal of Hazardous Materials 186 (2011) 1713–1719.
[38] L. Michot, I.A. Masion, F. Thomas, Mechanism of adsorption and desorption of water vapor by homoionic montmorillonites: 2. The Li^+, Na^+, K^+, Rb^+ and Cs^+-exchanged forms, Clays and Clay Minerals 43 (1995) 324–336.
[39] J. Koresh, A. Soffer, Application of the two-site Langmuir isotherm to microporous adsorbents, Journal of Colloid and Interface Science 92 (1983) 517–524.
[40] T. Gordon, A. Marsh, Temperature dependence of the oxidation of 2-chlorophenol by hydrogen peroxide in the presence of goethite, Catalysis Letters 132 (2009) 349–354.
[41] J. Chen, L. Zhu, Comparative study of catalytic activity of different Fe-pillared bentonites in the presence of UV light and H_2O_2, Separation and Purification Technology 67 (2009) 282–288.
[42] J.H. Ramirez, F.M. Duarte, F.G. Martins, C.A. Costa, L.M. Madeira, Modelling of the synthetic dye Orange II degradation using Fenton's reagent: from batch to continuous reactor operation, Chemical Engineering Journal 148 (2009) 394–404.
[43] J.H. Ramirez, C.A. Costa, L.M. Madeira, Experimental design to optimize the degradation of the synthetic dye Orange II using Fenton's reagent, Catalysis Today 107–108 (2005) 68–76.
[44] P.K. Malik, S.K. Saha, Oxidation of direct dyes with hydrogen peroxide using ferrous ion as catalyst, Separation and Purification Technology 31 (2003) 241–250.
[45] L.F. González-Bahamón, D.F. Hoyos, N. Benítez, C. Pulgarín, New Fe-immobilized natural bentonite plate used as photo-Fenton catalyst for organic pollutant degradation, Chemosphere 82 (2011) 1185–1189.